*Proc. Natl. Sci. Counc. ROC(A)*
Vol. 19, No. 5, 1995. pp. 378-386

# A Unified Analytical Model for the Phase-Controlled Rectifier with Voltage Source, Current Source, and DC Motor Loads

JUNG-CHIEN LI

*Department of Electrical Engineering*
*National Taiwan Ocean University*
*Keelung, Taiwan, R.O.C.*

(Received July 22, 1994; Accepted December 11, 1994)

**ABSTRACT**

We propose an analytical model which unifies the steady state analysis of a three-phase rectifier with voltage source, current source, and dc motor loads. The continuous conduction mode of the dc-side current is assumed, and the ac-side inductance which introduces the commutation effect is considered. The regulation curve of output voltage versus output current for the rectifier can be plotted on the output plane using the commutation angle as the parameter under some specified firing angle and dc-side inductance. The upper bound of the firing angle can be derived as a function of the dc-side inductance. The range of the commutation angle can be found as a function of the firing angle and the dc-side inductance. Then, the allowable operating region of the output plane for a certain dc-side inductance is determined.

**Key Words:** steady state analysis, continuous conduction mode, regulation curve

## I. Introduction

Ac-to-dc converters with SCRs as switching devices can (1) provide a constant voltage source via a dc-link capacitor (or an L-C filter) for a voltage source inverter or for a switching regulator, (2) provide a constant current source via a dc-link inductor for a current source inverter, or (3) supply an adjustable dc voltage to a dc drive motor (Mohan *et al.*, 1989; Bose, 1986; Krause, 1987). However, the dc-side current is generally assumed to be constant for simplified analysis (Kalra, 1990; Mohan *et al.*, 1989; Bose, 1986; Krause, 1987), which is not true for a voltage source load and for a dc motor load when the armature current is likely to be discontinuous at light loads.

All the above three kinds of loads can be modeled as the series connection of a constant voltage source, a resistance, and an inductance. In the case of a voltage source load, a dc-link capacitor with infinite capacitance exhibits a constant voltage source. The series inductance and resistance in the model can be zero if the filter inductor is not present. In the case of a current source load, the series inductance in the model is assumed to be infinite, since an infinite inductance presents a constant current source. In the case of a dc motor load, the back emf (proportional to the motor speed) is nearly constant because the mechanical time constant is much larger than the ripple period (one-sixth of the ac source period) on the dc side. The armature inductance and resistance act as the series inductance and resistance in the model.

A phase-controlled rectifier with load circuit characterized by a finite filter inductance in series with a constant voltage source was analyzed by Kwon (1992). However, the ac-side inductance, which adversely affects the commutation process, absorbs significant ac-side voltage drop, and reduces the output voltage especially at heavy loads, was not considered (Mohan *et al.*, 1989). In addition to the ac-side inductance, we consider the resistance associated with the dc-side inductance, which absorbs significant dc voltage drop at heavy loads. Since the ac voltage drop across the dc-side resistance is much less than that across the dc-side inductance and can be neglected, the load circuit is remodeled as another constant voltage source (original constant voltage source plus dc voltage drop across the dc-side resistance) in series with the inductance.

Given the value of this constant voltage source (known as the output voltage) in the load circuit, with continuity and periodicity of the dc-side current in steady state analysis, an auxiliary equation of the commutation angle can be derived. Furthermore, we can derive the average value (dc component) of the dc-side current, which is known as the output current. By

varying the commutation angle, the regulation curve of output voltage versus output current can be plotted on the output plane.

At light loads, the minimum value of the dc-side current waveform may approach zero, and the rectifier may enter the discontinuous conduction mode (DCM). The commutation angle, which increases as the output current increases, may become larger than $\pi/3$ (one ripple period on the dc side). For a rectifier operated in the inversion mode with a large firing angle, the output current should be limited to reduce the commutation angle, so that a sufficient turn-off time (margin angle) available to the SCRs is provided. To sum up, the above constraints can be combined to derive the operating range of the regulation curve, which depends on the firing angle and the dc-side inductance.

## II. Converter Analysis

The three-phase line-frequency phase-controlled rectifier is shown in Fig. 1, where $L_c$ is the commutating (ac-side) inductance, and $L_a$ and $e_d$ (a constant voltage source, which equals the dc component of $v$) form the model of the load circuit as described in the Introduction. Assume that $Q_3$ is triggered at $t=0$ with firing angle $\alpha$ to initiate a commutation interval in order to turn off $Q_1$. Then $v_{bc}=V_m\sin(w_st+\alpha+\pi/3)$, where $V_m$ is the peak value of the line-to-line voltage of the balanced ac source with an *abc* sequence, and $w_s$ is the angular frequency of the *ac* source. During the commutation interval $0\le t\le t_c$, Fig. 1 reduces to Fig. 2(a). Note that

$$i_a(0)=i(0),\ i_b(t_c)=i(t_c),\ i_a(t_c)=i_b(0)=0, \qquad (1)$$

which will be used in circuit analysis.

We derive the Thevenin equivalent circuit between $z$ and $y$ (left part), and Fig. 2(a) can be further simplified as Fig. 2(b), where $v_s=(v_{ac}+v_{bc})/2=(\sqrt{3}\,V_m/2)\cos(w_st+\alpha)$ and $L=L_a+3L_c/2$. We choose $V_m$ as the voltage base, $L_c$ as the inductance base, and $1/w_s$ as the time base. Then $w_sL_c$ becomes the impedance base, and $V_m/w_sL_c$ becomes the current base. Define $r=L_a/L_c$, $E=e_d/V_m$, $\Theta=w_st$, and $I=w_sL_ci/V_m$. Then $L/L_c=r+3/2\triangleq L_3$ and the normalized differential equation for Fig. 2(b) can be formulated as

$$L_3\frac{dI}{d\Theta}=\frac{\sqrt{3}}{2}\cos(\Theta+\alpha)-E,\quad 0\le\Theta\le\mu, \qquad (2)$$

where $\mu\triangleq w_st_c$ is the commutation angle, and $I(\Theta)$ can be solved as

$$I(\Theta:0\le\Theta\le\mu)=\frac{\sqrt{3}}{2L_3}\sin(\Theta+\alpha)-\frac{E\Theta}{L_3}+p, \qquad (3)$$

where $p$ is the constant of integration to be determined.

At $t=t_c$, $i_a=0$ and $Q_1$ is off. Then the equivalent circuit becomes Fig. 2(c). Define $T_r$ as the ripple period of $i(t)$, and we have $w_sT_r=\pi/3$. Therefore, Fig. 2(c) is

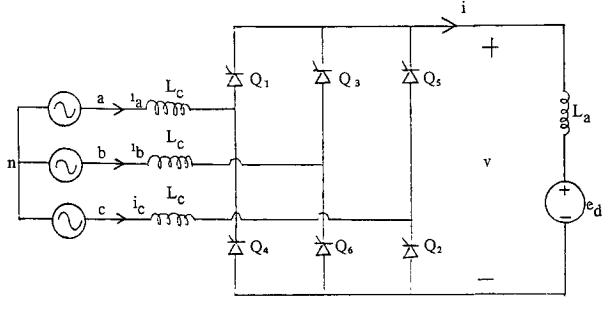


**Fig. 1.** Three-phase rectifier.

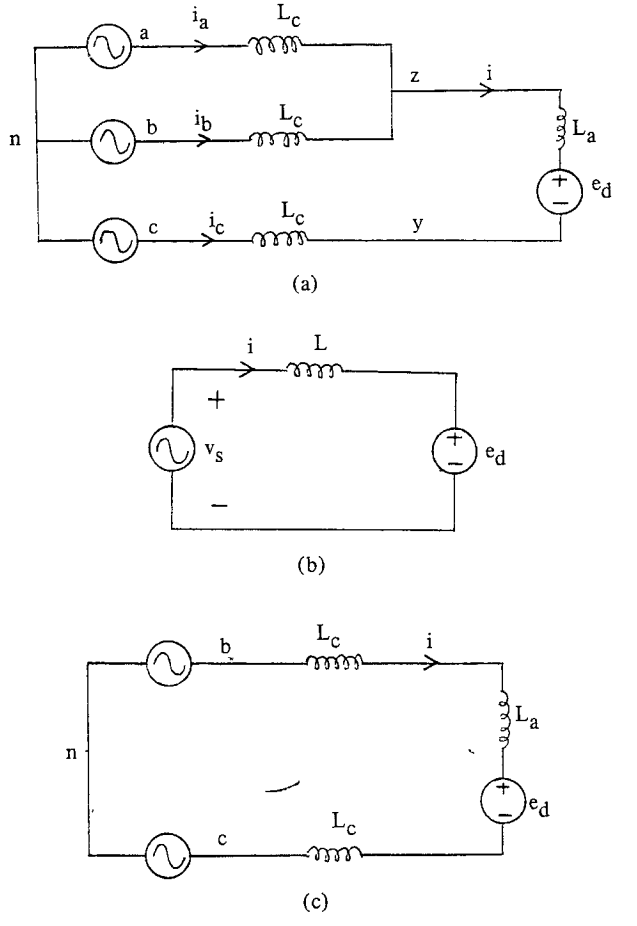


**Fig. 2.** (a) Equivalent circuit during commutation interval.
(b) Equivalent circuit of Fig.2(a).
(c) Equivalent circuit after the end of commutation.

valid during $\mu \le \Theta \le \pi/3$, and the normalized differential equation is

$$L_1 \frac{dI}{d\Theta} + E = \frac{v_{bc}}{V_m} = \sin\left(\Theta + \alpha + \frac{\pi}{3}\right), \quad \mu \le \Theta \le \frac{\pi}{3}, \quad \textbf{(4)}$$

where $L_1=(L_a+2L_c)/L_c=r+2$, and $I(\Theta)$ can be solved as

$$I\left(\Theta: \mu \le \Theta \le \frac{\pi}{3}\right) = \frac{-1}{L_1}\cos\left(\Theta + \alpha + \frac{\pi}{3}\right) - \frac{E}{L_1}\Theta + q, \quad \textbf{(5)}$$

where $q$ is the constant of integration to be determined. With continuity and periodicity of $I(\Theta)$ in steady state, we have $I(0)=I(\pi/3)$ and $I(\mu^-)=I(\mu^+)$, which lead to [using Eq. (3) and Eq. (5)]

$$\begin{aligned} p - q &= \frac{-1}{L_1}\cos\left(\alpha + \frac{2\pi}{3}\right) - \frac{\sqrt{3}\sin\alpha}{2L_3} - \frac{\pi E}{3L_1} \\ &= \frac{-1}{L_1}\cos\left(\mu + \alpha + \frac{\pi}{3}\right) - \frac{\sqrt{3}}{2L_3}\sin(\mu + \alpha) \\ &\quad + \frac{L_1 - L_3}{L_1 L_3} E\mu. \end{aligned} \quad \textbf{(6)}$$

During the commutation interval $0 \le t \le t_c$ in Fig. 2(a), the normalized differential equation is

$$\begin{aligned} \frac{dJ}{d\Theta} &= \frac{v_{ac}}{V_m} - E - \frac{L_a + L_c}{L_c}\frac{dI}{d\Theta} \\ &= [\text{using Eq. (2)}]\sin\left(\Theta + \alpha + \frac{2\pi}{3}\right) \\ &\quad - \frac{\sqrt{3}L_2}{2L_3}\cos(\Theta + \alpha) + \left(\frac{L_2}{L_3} - 1\right)E, \\ &\quad 0 \le \Theta \le \mu, \end{aligned} \quad \textbf{(7)}$$

where $J=w_s L_c i_a/V_m$ and $L_2=(L_a+L_c)/L_c=r+1$.

Equation (7) can be solved as

$$\begin{aligned} J\left(\Theta: 0 \le \Theta \le \mu\right) &= -\cos\left(\Theta + \alpha + \frac{2\pi}{3}\right) \\ &\quad - \frac{\sqrt{3}\,L_2}{2L_3}\sin(\Theta + \alpha) + \left(\frac{L_2}{L_3} - 1\right)E\Theta + M, \end{aligned} \quad \textbf{(8)}$$

where $M$ is the constant of integration to be determined with $I(0)=J(0)$ [from Eq. (1)] using Eq. (3) and Eq. (8). Then

$$M = (1 + L_2)\frac{\sqrt{3}\sin\alpha}{2L_3} + p + \cos\left(\alpha + \frac{2\pi}{3}\right). \quad \textbf{(9)}$$

Furthermore, using $J(\mu)=0$ [from Eq. (1) ] in Eq. (8) with $M$ given in Eq. (9), we obtain $p$, which can be substituted into Eq. (6) to give $q$ (using the first equality). The second equality of Eq. (6) indicates the auxiliary equation of the commutation angle $\mu$.

Using Eq. (3) and Eq. (5), we can obtain $\langle I \rangle$, the dc component of $I(\Theta)$, as

$$\begin{aligned} \langle I \rangle &= \frac{3}{\pi}\left[\int_0^{\mu} I(\Theta)\,d\Theta + \int_{\mu}^{\pi/3} I(\Theta)\,d\Theta\right] \\ &= \frac{3}{\pi}\left[-\frac{\sqrt{3}}{2L_3}\cos(\mu + \alpha) - \frac{E}{2L_3}\mu^2\right. \\ &\quad + p\mu + \frac{\sqrt{3}}{2L_3}\cos\alpha - \frac{1}{L_1}\sin\left(\alpha + \frac{2\pi}{3}\right) \\ &\quad - \frac{E}{2L_1}\left(\frac{\pi}{3}\right)^2 + \frac{\pi}{3}q + \frac{1}{L_1}\sin\left(\mu + \alpha + \frac{\pi}{3}\right) \\ &\quad \left. + \frac{E}{2L_1}\mu^2 - q\mu\right]. \end{aligned} \quad \textbf{(10)}$$

Therefore, $\langle I \rangle$ can be plotted as a function of $E$ for some firing angle $\alpha$.

However, from another viewpoint, we can solve $E(\mu)$ from Eq. (6) (using the second equality) as

$$\begin{aligned} E(\mu) &= \frac{3}{3\mu + \pi k}\left\{k\left[\cos\left(\mu + \alpha + \frac{\pi}{3}\right) - \cos\left(\alpha + \frac{2\pi}{3}\right)\right]\right. \\ &\quad \left. + \sqrt{3}\,(r+2)\left[\sin(\mu + \alpha) - \sin\alpha\right]\right\}, \end{aligned} \quad \textbf{(11)}$$

where $k=2r+3$. Substituting Eq. (11) for $E$ in the expressions of $p$ and $q$, we obtain $p(\mu)$ and $q(\mu)$. Using $p(\mu)$, $q(\mu)$, and $E(\mu)$ in Eq. (10), $\langle I \rangle$ can be obtained as a function of $\mu$. Thus, we can plot $E$ versus $\langle I \rangle$ by varying $\mu$ and obtain the regulation curve.

## III. Constraints for Commutation Angle $\mu$

When plotting the regulation curve, we must determine the range of $\mu$ in advance. We have $0<\mu<\pi/3$ and $I(\Theta)>0$ during $0 \le \Theta \le \pi/3$ in the continuous conduction mode (CCM). Equation (2) shows that, if $E>(\sqrt{3}/2)\cos\alpha$, then $I(\Theta)$ decreases monotonically during $0 \le \Theta \le \mu$, as illustrated in Fig. 3(a), where the area of the shaded region is proportional to the decrease in $I$. If $E<(\sqrt{3}/2)\cos\alpha$, then either $I(\Theta)$ increases monotonically during $0 \le \Theta \le \mu$, or $I(\Theta)$ first increases monotonically and then decreases monotonically during $0 \le \Theta \le \mu$, as illustrated in Fig. 3(b).

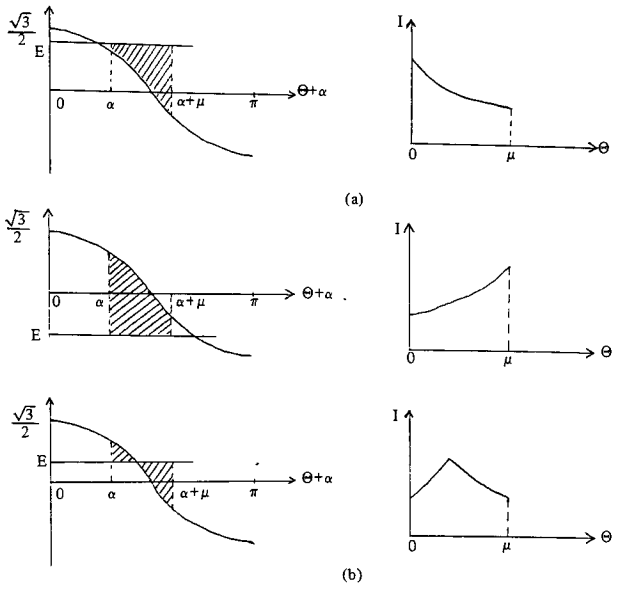


**Fig. 3.** (a) Illustration of (2) for $E>(\sqrt{3}/2)\cos\alpha$. (b) Illustration of (2) for $E<(\sqrt{3}/2)\cos\alpha$.

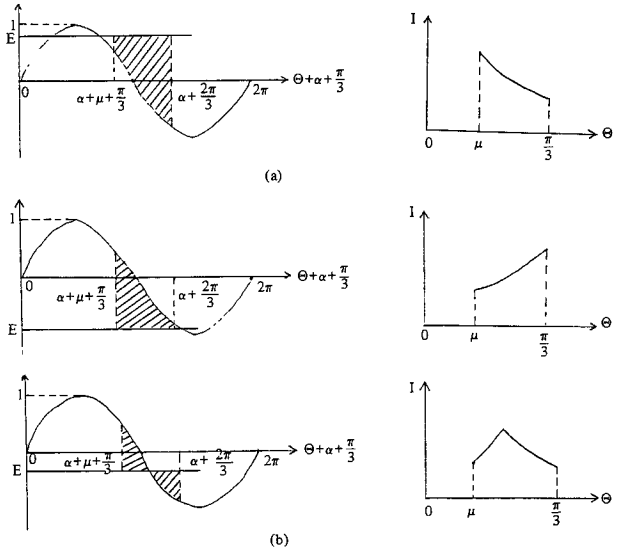


**Fig. 4.** (a) Illustration of (4) for $E>\sin(\alpha+\mu+\pi/3)$. (b) Illustration of (4) for $E<\sin(\alpha+\mu+\pi/3)$.

Equation (4) shows that, if $E>\sin(\mu+\alpha+\pi/3)$, then $I(\Theta)$ decreases monotonically during $\mu\le\Theta\le\pi/3$, as illustrated in Fig. 4(a). If $E<\sin(\mu+\alpha+\pi/3)$, then either $I(\Theta)$ increases monotonically during $\mu\le\Theta\le\pi/3$, or $I(\Theta)$ first increases monotonically and then decreases monotonically during $\mu\le\Theta\le\pi/3$, as illustrated in Fig. 4(b).

To summarize Fig. 3 and Fig. 4, we know that $\therefore$ $\mathrm{Min}[I(0), I(\mu), I(\pi/3)]=\mathrm{Min}[I(0), I(\mu)][\because I(0)=I(\pi/3)]$ gives the minimum value of $I(\Theta)$ during $0\le\Theta\le\pi/3$. Consequently, both $I(0)>0$ and $I(\mu)>0$ must be satisfied in the CCM.

We first consider $I(0)>0$. Using $p(\mu)$ in Eq. (3), we obtain

$$I(0)=\frac{\sqrt{3}\sin\alpha}{k}+p(\mu)$$

$$=\cos(\mu+\alpha+\frac{2\pi}{3})+F\cos(\mu+\alpha+\frac{\pi}{3})$$

$$-(1+F)\cos(\alpha+\frac{2\pi}{3})$$

$$+\frac{\sqrt{3}}{k}[\sin(\mu+\alpha)-\sin\alpha][r+1+(r+2)F], \quad (12)$$

where $F=3\mu/(3\mu+\pi k)$. Using trigonometric identities, Eq. (12) can be further simplified as

$$I(0)=A(r,\mu)\sin\alpha+B(r,\mu)\cos\alpha, \quad (13)$$

where

$$A(r,\mu)=-\sin(\mu+\frac{2\pi}{3})-F\sin(\mu+\frac{\pi}{3})+\frac{\sqrt{3}}{2}(1+F)$$

$$+\frac{\sqrt{3}}{k}(\cos\mu-1)[r+1+F(r+2)] \quad (14)$$

$$B(r,\mu)=\cos(\mu+\frac{2\pi}{3})+F\cos(\mu+\frac{\pi}{3})+\frac{1}{2}(1+F)$$

$$+\frac{\sqrt{3}}{k}(\sin\mu)[r+1+F(r+2)]. \quad (15)$$

Suppose that $A=R\cos\theta$ and $B=R\sin\theta$, where $R=\sqrt{A^2+B^2}$ and $\theta=\tan^{-1}(B/A)$. Then Eq. (13) can be further derived as $I(0)=R\sin(\alpha+\theta)$. $I(0)>0$ results in $0<\alpha+\theta<\pi$, and we have

$$-\alpha<\theta(r,\mu)<\pi-\alpha. \quad (16)$$

$\theta(r,\mu)$ can be plotted as a function of $\mu$ over $0\le\mu\le\pi/3$ for a fixed $r$. For some selected $\alpha$, (16) can be used to determine the allowable range of $\mu$.

From (14) and (15), $\mu=0$ results in $A=B=0$. Therefore,

$$\theta(r,0)\triangleq\lim_{\mu\to0}\theta(r,\mu)$$

$$=\tan^{-1}[\lim_{\mu\to0}\frac{B(r,\mu)}{A(r,\mu)}] \quad =(\text{using L'Hospital's rule})$$

$$\tan^{-1}(\frac{\partial B/\partial\mu}{\partial A/\partial\mu}\Big|_{\mu=0})=\tan^{-1}\frac{6-\sqrt{3}\pi}{\pi k}>0. \quad (17)$$

Using Eq. (14) and Eq. (15),

$$\theta(r,\frac{\pi}{3})=\tan^{-1}\frac{B(r,\pi/3)}{A(r,\pi/3)}=\frac{\pi}{6}>0. \quad (18)$$

Now we consider the second restriction $I(\mu)>0$ for the CCM. Using Eq. (11) and $p(\mu)$ in Eq. (3), we obtain

$$I(\mu)=\frac{\sqrt{3}}{k}\sin(\mu+\alpha)-\frac{2E(\mu)\mu}{k}+p(\mu)$$

$$=\frac{\sqrt{3}}{k}(r+2)(1-F)[\sin(\mu+\alpha)-\sin\alpha]$$

$$+(F-1)\cos(\alpha+\frac{2\pi}{3})+\cos(\mu+\alpha+\frac{2\pi}{3})$$

$$-F\cos(\mu+\alpha+\frac{\pi}{3}), \quad (19)$$

which can be further simplified as [similar to Eq. (12) -Eq. (15)]

$$I(\mu)=C(r,\mu)\sin\alpha+D(r,\mu)\cos\alpha, \quad (20)$$

where

$$C(r,\mu)=\frac{\sqrt{3}}{k}(r+2)(1-F)(\cos\mu-1)$$

$$+\frac{\sqrt{3}}{2}(1-F)-\sin(\mu+\frac{2\pi}{3})$$

$$+F\sin(\mu+\frac{\pi}{3}) \quad (21)$$

$$D(r,\mu)=\frac{\sqrt{3}}{k}(r+2)(1-F)\sin\mu+\frac{1}{2}(1-F)$$

$$+\cos(\mu+\frac{2\pi}{3})-F\cos(\mu+\frac{\pi}{3}). \quad (22)$$

Define $\phi=\tan^{-1}(D/C)$. As the derivation for (16), $I(\mu)>0$ results in

$$-\alpha<\phi(r,\mu)<\pi-\alpha. \quad (23)$$

From Eqs. (21) and (22), $\mu=0$ results in $C=D=0$. Therefore,

$$\phi(r,0)\triangleq\lim_{\mu\to 0}\phi(r,\mu)$$

$$=\tan^{-1}\left(\frac{\partial D/\partial\mu}{\partial C/\partial\mu}\Big|_{\mu=0}\right)=\tan^{-1}\frac{\sqrt{3}\pi-6}{\pi k}$$

$$=[\text{see Eq. (17)}]-\theta(r,0)<0. \quad (24)$$

Using Eqs. (21) and (22),

$$\phi(r,\frac{\pi}{3})=\tan^{-1}\frac{D(r,\pi/3)}{C(r,\pi/3)}=\frac{\pi}{6}$$

$$=[\text{see Eq. (18)}]\,\theta(r,\frac{\pi}{3})>0. \quad (25)$$

When the firing angle $\alpha$ becomes larger (more than $\pi/2$), we must check whether there is a sufficient turn-off time available to the SCRs. Compare Fig. 2(a) with Fig. 1, and note that after $\theta=\mu$ ($Q_1$ turns off and $i_a=0$), $v_{az}$ is the voltage across $Q_1$. Then we have

$$v_{az}=v_{ab}+L_c\frac{di_b}{dt}=v_{ab}+L_c\frac{di}{dt}. \quad (26)$$

We normalize Eq. (26), substitute $dI/d\Theta$ from Eq. (4), and obtain

$$\frac{v_{az}(\Theta)}{V_m}=-\sin(\Theta+\alpha)$$

$$+\frac{1}{r+2}[\sin(\Theta+\alpha+\frac{\pi}{3})-E]. \quad (27)$$

Let $t_q$ be the required turn-off time for the SCRs. To ensure the turn-off of $Q_1$, we must have $v_{az}(\mu+w_st_q)<0$. From Mohan *et al.* (1989), $w_st_q=15°$ to $30°$ for $w_s=377$ rad/s. For a conservative design, select $w_st_q=\pi/6$ rad.

Using Eq. (27), $v_{az}(\mu+\pi/6)<0$ leads to

$$E>\cos(\mu+\alpha)-(r+2)\sin(\mu+\alpha+\frac{\pi}{6}). \quad (28)$$

Substituting Eq. (11) into Eq. (28) with simplification gives

$$G(r,\mu)\sin\alpha+H(r,\mu)\cos\alpha>0, \quad (29)$$

where

$$G(r,\mu)=-\frac{k}{2}\sin\mu+\frac{\sqrt{3}}{2}(\cos\mu-1)$$

$$+\frac{3\mu+\pi k}{3}[\frac{\sqrt{3}}{2}(r+2)\cos\mu-\frac{r}{2}\sin\mu] \quad (30)$$

$$H(r,\mu)=\frac{\sqrt{3}}{2}\sin\mu+\frac{k}{2}(\cos\mu+1)$$

$$+\frac{3\mu+\pi k}{3}[\frac{\sqrt{3}}{2}(r+2)\sin\mu+\frac{r}{2}\cos\mu]. \quad (31)$$

Define $\psi=\tan^{-1}(H/G)$. Then Eq. (29) leads to [as the

derivation for Eq. (16)]

$$-\alpha<\psi(r,\ \mu)<\pi-\alpha. \tag{32}$$

Using Eqs. (30) and (31),

$$\psi(r,0)=\tan^{-1}\frac{H(r,0)}{G(r,0)}=\tan^{-1}\frac{\pi r+6}{\sqrt{3}\pi(r+2)}>0 \tag{33}$$

$$\psi(r,\frac{\pi}{3})=\tan^{-1}\frac{H(r,\pi/3)}{G(r,\pi/3)}=\tan^{-1}\frac{2\pi k+9}{\sqrt{3}(2\pi-3)}>0. \tag{34}$$

For given $r(>0)$ and $\alpha(>0)$, $\mu$ must satisfy $0<\mu<\pi/3$, Eqs. (16), (23), and (32) simultaneously. $\theta(r,\ \mu)$, $\phi(r,\ \mu)$, and $\psi(r,\ \mu)$ are all increasing functions of $\mu$. $\phi(r,\ \mu)$ and $\psi(r,\ \mu)$ are both increasing functions of $r$ whereas $\theta(r,\ \mu)$ is a decreasing function of $r$. The above arguments are illustrated in Fig. 5, where Fig. 5(b) exhibits exactly two straight lines, which will be discussed later in Eqs. (37) and (38). The reader can also check Eqs. (17), (18), (24), (25), (33), and (34) in Fig. 5 and see how $r$ affects the plots. It can be easily seen that

$$\phi(r,\ \mu)<\theta(r,\ \mu)<\psi(r,\ \mu). \tag{35}$$

Therefore, Eqs. (16), (23), (32), and (35) can be combined to give

$$\phi(r,\ \mu)>-\alpha \text{ and } \psi(r,\ \mu)<\pi-\alpha, \tag{36}$$

which can be used to determine the range of $\mu$ for given $r$ and $\alpha$. $\phi(r,\ \mu)>-\alpha$ determines $\mu_{min}$ while $\psi(r,\ \mu)<\pi-\alpha$ determines $\mu_{max}$, which is illustrated in Fig. 6, where $(\pi-\alpha)-(-\alpha)=\pi$ is constant and independent of $\alpha$.

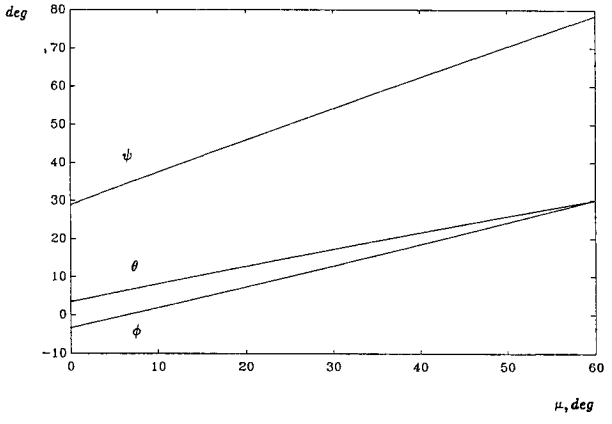


(a)

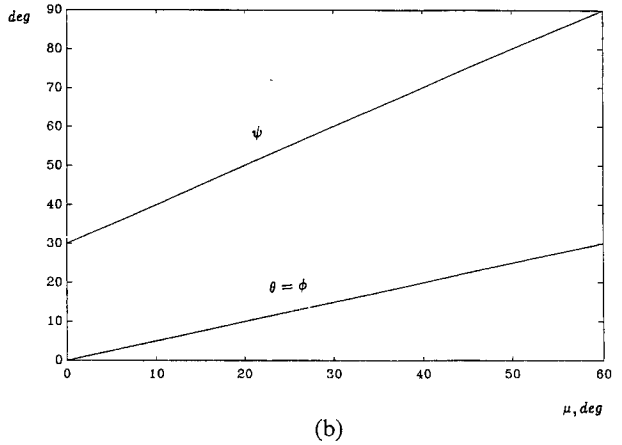


(b)

**Fig. 5.** (a) The limiting case of $\theta(r,\ \mu)$, $\phi(r,\ \mu)$, and $\psi(r,\ \mu)$ for $r=0$.
(b) The limiting case of $\theta(r,\ \mu)$, $\phi(r,\ \mu)$, and $\psi(r,\ \mu)$ for $r\to\infty$.

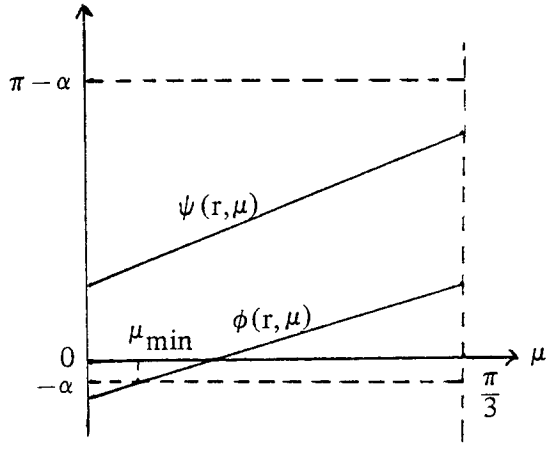


(a)

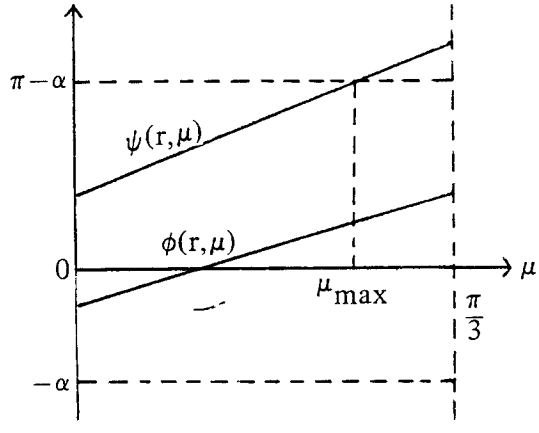


(b)

**Fig. 6.** Graphical illustration of $\mu_{min}$ and $\mu_{max}$; (a) small $\alpha$, (b) large $\alpha$.

The limiting case of $r\to\infty$ indicates a constant current source load on the dc side, which is normally assumed in classical studies. Using Eqs. (14) and (15),

$$\theta(\infty,\mu)=\tan^{-1}\left(\frac{1-\cos\mu}{\sin\mu}\right)=\tan^{-1}\left(\tan\frac{\mu}{2}\right)=\frac{\mu}{2}. \tag{37}$$

Using Eqs. (21) and (22), we similarly obtain $\phi(\infty, \mu)=\mu/2$. $\theta(\infty, \mu)=\phi(\infty, \mu)$ is not surprising because $I(0)=I(\mu)$ for constant $I(\Theta)$, which leads to $A(\infty, \mu)=C(\infty, \mu)$ and $B(\infty, \mu)=D(\infty, \mu)$ in Eqs. (13) and (20).

Using Eqs. (30) and (31), we obtain

$$\psi(\infty,\mu)=\tan^{-1}\left(\frac{\sqrt{3}\sin\mu+\cos\mu}{\sqrt{3}\cos\mu-\sin\mu}\right)$$

$$=\tan^{-1}\left[\frac{\sin(\mu+\pi/6)}{\cos(\mu+\pi/6)}\right]=\mu+\frac{\pi}{6}. \tag{38}$$

Recall that $w_s t_q=\pi/6$. In the foregoing derivation for $\psi(r, \mu)$, if $\pi/6$ is not substituted for $w_s t_q$, and $r$ is assumed to be infinite, we obtain $\psi(\infty, \mu)=\mu+w_s t_q$. Since $\psi(\infty, \mu)<\pi-\alpha$ in Eq. (36), we have $\pi-\alpha-\mu>w_s t_q$, which is consistent with classical results.

## IV. Operating Range and Output Plane

We are going to compute the allowable range of $\alpha$ and the range of $\mu$ for a given $\alpha$. $\alpha_{\min}=0$ is self-explanatory. From Fig. 6(b), we can see that $\pi-\alpha_{\max}=\psi(r, 0)$ while $\mu_{\max}=0=\mu$. From Fig. 6(b), if $\pi-\alpha>\psi(r, \pi/3)$, we have $\mu_{\max}=\pi/3$. From Fig. 6(a), if $-\alpha<\phi(r, 0)$, we have $\mu_{\min}=0$. We summarize the above arguments in Table 1.

However, as Fig. 5 and Eq. (24) show, we have $\phi(r, 0)\approx 0$, and the third row of Table 1 can be eliminated. Thus, the operating regions are illustrated in Fig. 7, where Region I and Region II correspond to the first and the second rows of Table 1, respectively.

From Fig. 5 and Eq. (33), $\psi(r, 0)\approx\pi/6$, and $\psi(r, \mu)$ is nearly a straight line. Therefore, using Eq. (34), we have

**Table 1.** Range of Commutation Angle $\mu$ for Different Regions of Firing Angle $\alpha$

| | | |
|---|---|---|
| $\pi-\psi(r, \frac{\pi}{3})<\alpha<\alpha_{\max}$<br>$\alpha_{\max}=\pi-\psi(r, 0)$ | : | $0=\mu_{\min}\le\mu\le\mu_{\max}<\frac{\pi}{3}$<br>$\psi(r, \mu_{\max})=\pi-\alpha$ |
| $-\phi(r, 0)<\alpha<\pi-\psi(r, \frac{\pi}{3})$ | : | $0=\mu_{\min}\le\mu\le\mu_{\max}=\frac{\pi}{3}$ |
| $0=\alpha_{\min}<\alpha<-\phi(r, 0)$ | : | $0<\mu_{\min}\le\mu\le\mu_{\max}=\frac{\pi}{3}$<br>$\phi(r, \mu_{\min})=-\alpha$ |

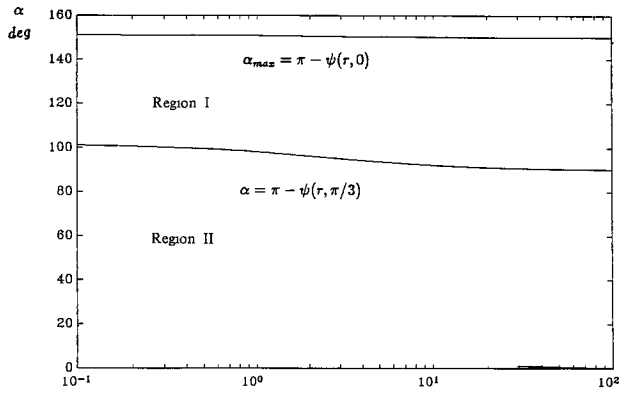


**Fig. 7.** Operating regions of the firing angle $\alpha$ as a variation of the normalized dc-side inductance $r$.

$$\psi(r,\mu)\approx\frac{\pi}{6}+\frac{3}{\pi}\left\{\left[\tan^{-1}\frac{2\pi k+9}{\sqrt{3}(2\pi-3)}\right]-\frac{\pi}{6}\right\}\mu. \tag{39}$$

From $\psi(r, \mu_{\max})=\pi-\alpha$, we obtain

$$\mu_{\max}\approx\frac{\frac{5\pi}{6}-\alpha}{\frac{3}{\pi}\left[\tan^{-1}\frac{2\pi k+9}{\sqrt{3}(2\pi-3)}\right]-\frac{1}{2}} \tag{40}$$

for Region I. Note that $\alpha_{\max}=\pi-\psi(r, 0)\approx 5\pi/6$, as can be verified in Fig. 7.

Now consider the limiting case of $r\to\infty$, which also results in $k\to\infty$, $L_1\to\infty$, $L_2\to\infty$, and $L_3\to\infty$. Equation (11) can be simplified as

$$E=\frac{3}{\pi}\left[\cos\left(\mu+\alpha+\frac{\pi}{3}\right)-\cos\left(\alpha+\frac{2\pi}{3}\right)\right]$$

$$+\frac{3\sqrt{3}}{2\pi}\left[\sin(\mu+\alpha)-\sin\alpha\right]$$

$$=\frac{3}{2\pi}\left[\cos\alpha+\cos(\mu+\alpha)\right]. \tag{41}$$

Equation (10) can be simplified as

$$<I>=\frac{3}{\pi}p\mu+q\left(1-\frac{3}{\pi}\mu\right). \tag{42}$$

From Eq. (6) (using the first equality), $p=q$. We have derived $p$ by using Eqs. (8) and (9). Then Eq. (42) results in

$$<I>=p=\frac{\sqrt{3}}{2}\left[\sin(\mu+\alpha)-\sin\alpha\right]$$

$$+\cos(\mu+\alpha+\frac{2\pi}{3})-\cos(\alpha+\frac{2\pi}{3})$$

$$=\frac{1}{2}[\cos\alpha-\cos(\mu+\alpha)]. \quad \textbf{(43)}$$

From Eq. (43), we obtain $\cos(\mu+\alpha)$, which is substituted into Eq. (41) to yield

$$E=\frac{3}{\pi}(\cos\alpha-<I>). \quad \textbf{(44)}$$

Equations (43) and (44) are consistent with classical results (Mohan *et al.*, 1989).

Figure 8 illustrates three families of regulation curves of $E$ versus $<I>$ on the output planes by varying $0°\le\mu\le\mu_{max}$ for $\alpha$=0°, 30°, 60°, 90°, 120°, and 150° with $r$=0, 10, and ∞. Each additional symbol * to the right indicates a 10° increase of $\mu$. Once the operating point is determined, the corresponding $\mu$ can be found by linear interpolation. Note that for $r\to\infty$ and $\alpha$=150°, we have $\mu$=0°[$\psi(\infty, \mu_{max})=\pi-\alpha\Rightarrow\mu_{max}$=0° by using Eq. (38)], $<I>$=0 [from Eq. (43)], and $E=-3\sqrt{3}/2\pi=-0.827$ [form Eq. (44)], which is just a point and is not indicated in Fig. 8(c). The left dashed curve, the right dashed curve, the upper regulation curve, and the lower regulation curve on each output plane of Fig. 8 enclose the region in which the operating point is allowed to exist. $<I>_{min}$=0 in Fig. 8(c) because a constant current always remains in the CCM, and the left dashed curve is just the vertical axis. Figure 8 agrees with the steady-state solution obtained from the transient simulation with 12 rectifier topological modes in an ac source period.

## V. Discussions

Figure 8(b) is similar to Fig. 8(c), which means that for $r\ge$10, the dc side can be well approximated by a constant current source. This can also be seen in Fig. 7, where the boundary curve $\alpha=\pi-\psi(r, \pi/3)$ is almost a horizontal line in $10\le r\le 100$. For a large firing angle $\alpha$, the commutation angle $\mu$ cannot be large (see Fig. 8) as to provide a sufficient turn-off time available to the SCRs, and the normalized output current $<I>$ is thus limited.

As the normalized dc-side inductance $r$ becomes smaller, $<I>_{min}$ becomes larger, as illustrated by the three left dashed curves of Fig. 8. This can be explained as follows. As $r$ becomes smaller, the dc-side current waveform $I(\Theta)$ has more ripple, and the minimum value of $I(\Theta)$ may go negative. Consequently, $<I>$ [dc component of $I(\Theta)$] must be larger to raise the minimum value of $I(\Theta)$ above zero so as to avoid entering the DCM.

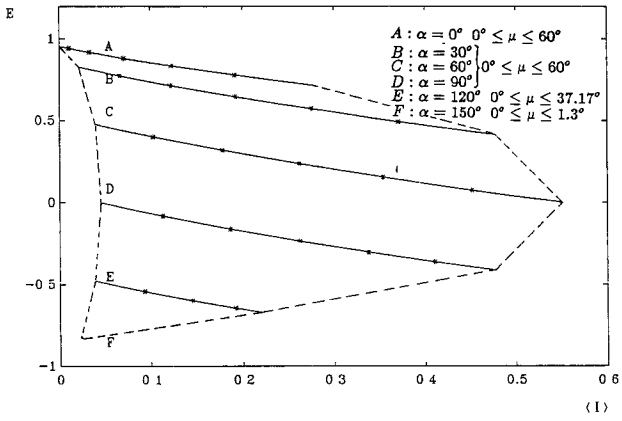


(a)

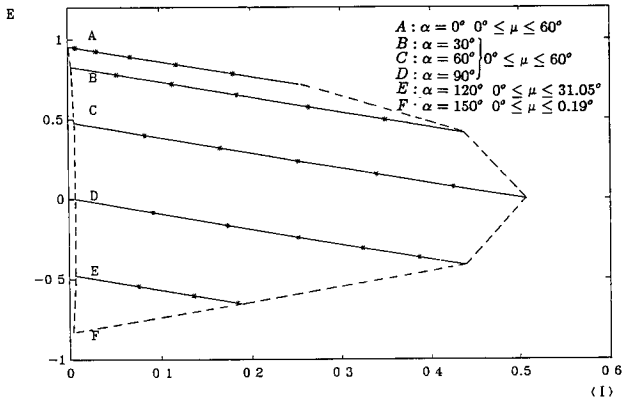


(b)

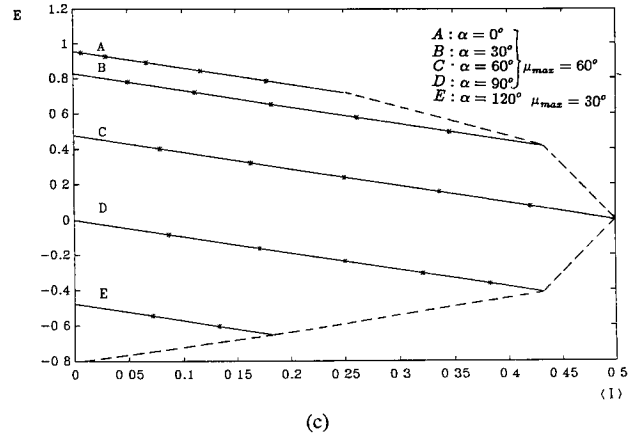


(c)

**Fig. 8.** (a) Regulation curves for $r$=0.
(b) Regulation curves for $r$=10.
(c) Regulation curves for $r\to\infty(\mu_{min}=0°)$.

## VI. Conclusions

An analytical model with all equations and variables normalized has been presented for a rectifier circuit with voltage source, current source, and dc motor loads, which are all modeled as the series con-

nection of an inductance, a resistance, and a constant voltage source. We neglect the ac voltage across the resistance and obtain another constant voltage source in series with the inductance on the dc side. With a positive-sequence balanced three-phase ac voltage source in series with the commutating inductances on the ac side , we have been able to perform periodic steady-state waveform analysis in the CCM and derive regulation curves on the output plane, whose allowable operating region is determined under a certain dc-side inductance.

## References


Bose, B. K. (1986) *Power Electronics and AC Drives*. Prentice-Hall, Englewood Cliffs, NJ, U.S.A.

Dubey, G. K. (1989) *Power Semiconductor Controlled Drives*. Prentice-Hall, Englewood Cliffs, NJ, U.S.A.

Erickson, R., M. Madigan, and S. Singer (1990) Design of a simple high-power-factor rectifier based on the flyback converter. *IEEE Applied Power Electronics Conference*, 792-801.

Kalra, P. K. (1990) An approach for handling the nonlinearities of HVDC system for stability analysis. *IEEE Trans. on Power Electronics*, **5**(3),371-377.

Krause, P. C. (1987) *Analysis of Electric Machinery*. McGraw-Hill, Singapore.

Kwon, B. H. (1992) Design of a highly stable electromagnet power supply. *IEEE Trans. on Industrial Electronics*, **39**(2),149-158.

Mohan, N., T. M. Undeland, and W. P. Robbins (1989) *Power Electronics: converters, applications and design*. Wiley, New York, NY, U.S.A.

Slemon, G. R. (1992) *Electric Machines and Drives*. Addison-Wesley, Sydney, Australia.

Wernekinck, E., A. Kawamura, and R. Hoft (1991) A high frequency ac/dc converter with unity power factor and minimum harmonic distortion. *IEEE Trans. on Power Electronics*, **6**(3), 364-370.


# 相位控制整流器對於電壓源、電流源與直流馬達負載的統一解析模型


李榮乾

台灣海洋大學電機工程系所


## 摘　要


我們對於具有電壓源、電流源、與直流馬達負載的三相整流器提出其穩態分析的統一解析模型。我們假設直流側電流爲連續導通模式並考慮引起換向效應的交流側電感。對於某特定觸發角與直流側電感，我們使用換向角爲參數在輸出平面上畫出整流器輸出電壓對輸出電流的調整曲線。觸發角的上限可推導爲直流側電感的函數。換向角的範圍可推導爲觸發角與直流側電感的函數。因此對於某特定直流側電感，我們可求得輸出平面上的允許操作區域。